Available online at www.sciencedirect.com
ScienceDirect
Geochimica et Cosmochimica Acta 71 (2007) 5155–5167
Geochimica et Cosmochimica Acta
www.elsevier.com/locate/gca

Formation of iron sulfide nodules during anaerobic oxidation of methane

Bart E. van Dongen [a,*], Andrew P. Roberts [b], Stefan Schouten [c], Wei-Teh Jiang [d], Fabio Florindo [e], Richard D. Pancost [a]

[a] Organic Geochemistry Unit, Bristol Biogeochemistry Research Centre, School of Chemistry, Cantock's Close, Bristol University, Bristol BS8 1TS, United Kingdom
[b] National Oceanography Centre, University of Southampton, European Way, Southampton SO14 3ZH, United Kingdom
[c] Department of Marine Biogeochemistry, Royal Netherlands Institute for Sea Research, P.O. Box 59, 1790 AB Den Burg, Texel, The Netherlands
[d] Department of Earth Sciences, National Cheng Kung University, Tainan 70101, Taiwan, Republic of China
[e] Istituto Nazionale di Geofisica e Vulcanologia, Via di Vigna Murata, 605, I-00143 Rome, Italy

Received 20 October 2006; accepted in revised form 31 August 2007; available online 18 September 2007

Abstract

The biomarker compositions of iron sulfide nodules (ISNs; upper Pliocene Valle Ricca section near Rome, Italy) that contain the ferrimagnetic mineral greigite (Fe_3S_4) were examined. In addition to the presence of specific terrestrial and marine biomarkers, consistent with formation in coastal marine sediments, these ISNs contain compounds thought to originate from sulfate reducing bacteria (SRB). These compounds include a variety of low-molecular-weight and branched alkanols and several non-isoprenoidal dialkyl glycerol diethers (DGDs). In addition, archaeal biomarkers, including archaeol, macrocyclic isoprenoidal DGDs and isoprenoidal glycerol dialkyl glycerol tetraethers are also present. Both SRB and archaeal lipid $\delta^{13}C$ values are depleted in ^{13}C ($\delta^{13}C$ values are typically less than $-50‰$), which suggests that the SRB and archaea consumed ^{13}C depleted methane. These biomarker and isotopic signatures are similar to those found in cold seeps and marine sediments where anaerobic oxidation of methane (AOM) occurs with sulfate serving as the terminal electron acceptor. Association of AOM with formation of greigite-containing ISNs could provide an explanation for documented remagnetization of the Valle Ricca sediments. Upward migration of methane, subsequent AOM and associated authigenic greigite formation are widespread processes in the geological record that have considerable potential to compromise paleomagnetic records.

1. INTRODUCTION

Ferrimagnetic iron oxides are usually a minor but common component of marine sediments and are important carriers of paleomagnetic information. The reliability of the recovered paleomagnetic information depends on the validity of the assumption that the magnetic signal was acquired at or near the time of deposition. This assumption does not always hold. For instance, ferrimagnetic magnetite (Fe_3O_4), which is the most common terrestrial magnetic mineral, can be altered to paramagnetic pyrite (FeS_2; e.g. Berner, 1970) during anoxic diagenesis. Magnetite dissolution is the major cause of the destruction of paleomagnetic records in marine sediments (Karlin and Levi, 1983, 1985; Canfield and Berner, 1987; Channell and Hawthorne, 1990; Karlin, 1990; Passier et al., 1998). The hydrogen sulfide needed for formation of iron sulfides in anoxic environments is produced via bacterial reduction of sulfate (SO_4^{2-}), which enables biogenic oxidation of organic

* Corresponding author. Present address: School of Earth, Atmospheric and Environmental Sciences, University of Manchester, Williamson Building, Oxford Road, Manchester M13 9PL, United Kingdom. Fax: +44 1613069361.
E-mail address: Bart.vandongen@manchester.ac.uk (B.E. van Dongen).

0016-7037/$ - see front matter © 2007 Elsevier Ltd. All rights reserved.
doi:10.1016/j.gca.2007.08.019

matter (OM) by anaerobic microorganisms. Hydrogen sulfide can also be produced during anaerobic oxidation of methane (CH_4; AOM; Goldhaber, 2003; Burdige, 2006). Molecular, isotopic, and molecular biological approaches have revealed that AOM is performed by consortia of methanotrophic archaea and sulfate reducing bacteria (SRB; e.g. Hinrichs et al., 1999; Boetius et al., 2000; Thiel et al., 2001). The coupled reaction is proposed to proceed according to the following equation (Murray et al., 1978; Devol and Ahmed, 1981; Niewöhner et al., 1998):

$$CH_4 + SO_4^{2-} \rightarrow HCO_3^- + HS^- + H_2O \quad (1)$$

The depth of the horizon where this reaction occurs, the sulfate/methane transition zone (SMTZ), depends on: (i) the penetration depth of seawater sulfate into the sediment, and (ii) the intensity of the methane flux from deeper sediment layers. Recent studies indicate that a distinct magnetic susceptibility minimum can coincide with this SMTZ (Garming et al., 2005; Riedinger et al., 2005), which indicates that the released HS^- reacts with and causes dissolution of magnetite and results in precipitation of paramagnetic pyrite. In other cases, a susceptibility peak has been observed at the SMTZ, and this has been attributed to precipitation of ferrimagnetic greigite, the intermediate reaction product of pyritization reactions (Neretin et al., 2004). The formation of either pyrite or greigite depends largely on the availability of hydrogen sulfide. Generally, limited hydrogen sulfide availability favors greigite formation, whereas higher concentrations favor production of the more stable pyrite (Kao et al., 2004). Greigite is a thiospinel (Skinner et al., 1964) that shares the same crystal structure as magnetite and is therefore strongly ferrimagnetic. Thus, greigite formation and preservation can produce a strong paleomagnetic signal during diagenesis (Roberts and Turner, 1993; Florindo and Sagnotti, 1995; Kasten et al., 1998; Jiang et al., 2001; Neretin et al., 2004; Roberts and Weaver, 2005), which complicates sedimentary paleomagnetic records. However, although multiple mechanisms have been proposed for sedimentary remagnetizations involving greigite (Roberts and Weaver, 2005, and references therein), many details associated with these mechanisms remain unclear.

The potential role of AOM suggests that bacterial and archaeal lipid biomarkers could provide insights into iron sulfide nodule (ISN) formation. A wide range of biomarkers, including fatty acids, isoprenoidal and non-isoprenoidal ether lipids and hopanoids have all been reported in cold seeps and have been used to reconstruct microbiological processes (Hinrichs et al., 1999, 2000; Thiel et al., 1999, 2001; Hinrichs et al., 2000; Pancost et al., 2000, 2001a,b; Peckmann and Thiel, 2004; Werne et al., 2004; Orcutt et al., 2005). The biomarker approach is particularly powerful when studying AOM because biomarker $\delta^{13}C$ values can be used to evaluate cycling of ^{13}C-depleted methane (Pancost and Sinninghe Damsté, 2003). Thus, the goals of our study were to determine whether: (a) OM and biomarkers are preserved in sedimentary iron sulfides; (b) preserved biomarkers provide information on the depositional environment and microbial assemblages associated with ISN formation; and (c) the carbon isotopic compositions of these biomarkers provide evidence that the sulfide nodules were formed in association with AOM. Additionally, we have routinely observed strongly magnetic macroscopic ISNs in our studies of sulfidic sediments (e.g. Jiang et al., 2001; Weaver et al., 2002; Roberts and Weaver, 2005; Rowan and Roberts, 2006), which suggests that such nodules commonly form in sulfidic sediments. There is no direct evidence to assume that any of these environments were cold seeps. Recent research suggests that methane migration can cause formation of nodular aggregates of magnetic iron sulfide minerals (Larrasoaña et al., 2007) in settings where the full suite of diagenetic environments down to methanic have been experienced, and where tectonically forced fluid migration has disrupted the normal steady state diagenetic progression and has provided reactants for later than normal formation of these iron sulfides. Such nodules can potentially occur where there is enough OM, Fe and sulfide to enable their precipitation (i.e. during early diagenesis/earliest burial or in response to a range of later fluid migration events as indicated by Roberts and Weaver (2005)). Organic geochemistry is a powerful tool for discriminating between such options and for potentially explaining why the studied sediments have been remagnetized, which provides further motivation for undertaking the present study of ISNs from a remagnetized sediment.

2. METHODS

2.1. Study area and sampling

The studied ISNs (Fig. 1) were collected from the upper Pliocene Valle Ricca section in the Tini quarry, about 15 km northeast of Rome, close to the village of Monterotondo. Previous studies provide a detailed description of the sedimentary succession (Florindo and Sagnotti, 1995; Borzi et al., 1998; Di Bella et al., 2005). The nodules were found on an east-facing outcrop within strata that lie approximately 10 m above the ash layer in the sequence described

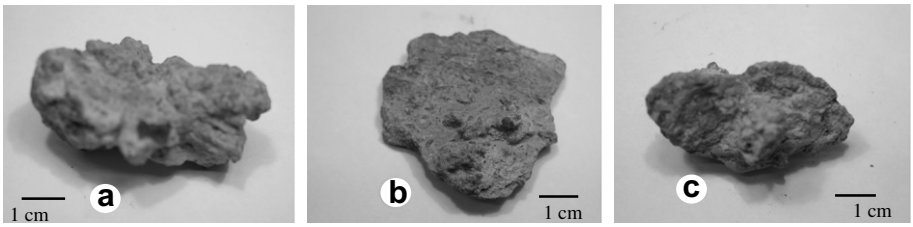

Fig. 1. Photographs of iron sulfide nodules obtained from the upper Pliocene Valle Ricca section, Italy.

by Florindo and Sagnotti (1995). Nodules from this locality were previously studied by Bracci et al. (1985), who reported X-ray diffraction (XRD) data that clearly indicate the presence of greigite.

2.2. Extraction and fractionation of organic compounds

Three ISNs (Fig. 1), with dimensions of approximately $2 \times 4 \times 1$ cm, were rinsed with dichloromethane (DCM), dried and crushed. Small amounts of material were used for elemental analyses and the remaining material was used for biomarker analyses. The samples were extracted using a Soxhlet apparatus with dichloromethane/methanol (DCM/MeOH, 2:1, v/v) for 24 h, and the total lipid extracts (TLE) were concentrated using rotary evaporation. An aliquot of the TLE was treated with activated (2 N HCl) copper curls to remove elemental sulfur, and a mixture of three standards (androstane, hexadecan-2-ol and hexadecyl-1-octadecanoate) was added. Subsequently, the aliquots were separated into three fractions using a column (pasteur pipette) packed with 2–3 cm (activated) alumina by elution with hexane (3 ml; ''saturated hydrocarbon fraction''), hexane/DCM (9:1 v/v; 3 ml; ''aromatic hydrocarbon fraction'') and DCM/MeOH (1:1 v/v; 3 ml; ''polar fraction''). The saturated hydrocarbon and polar fractions were analysed using gas chromatography (GC), gas chromatography/mass spectrometry (GC/MS), and gas chromatography combustion isotope-ratio mass spectrometry (GC/C/IRMS). Prior to analysis, the polar fraction was dissolved in 25 μl pyridine with 25 μl bis(trimethylsilyl)trifluoroacetamide (BSTFA) and heated (70 °C; 60 min) to convert alcohols into their corresponding trimethylsilyl ethers.

Analyses of the intact glycerol dialkyl glycerol tetraethers (GDGTs) were carried out on the polar fraction using a method similar to that reported by Hopmans et al. (2004). In short, the polar fractions were dissolved in hexane/isopropanol (99:1 v/v) and filtered using a 0.45 μm, 4 mm diameter polytetrafluoroethylene filter. The filtered fractions were analysed using high-performance liquid chromatography atmospheric pressure chemical ionization mass spectrometry (HPLC-APCI-MS).

2.3. Instrumental analyses

The bulk mineralogy of the studied ISNs, as reported in Fig. 2a, was investigated by subjecting crushed samples to XRD using a Philips X-ray diffractometer with Co-Kα radiation at the National Oceanography Centre, Southampton (NOCS). The petrography of the nodules was investigated at NOCS using a Leo 1450VP scanning electron microscope (SEM) operated at 15 keV. Elemental analyses were obtained using a Princeton Gamma Tech (IMIX-PTS) energy dispersive spectrometer (EDS) with a 2–3 μm diameter X-ray beam. With careful analysis it is possible to distinguish between a range of iron sulfide species using an EDS system (e.g. Jiang et al., 2001; Weaver et al., 2002; Roberts and Weaver, 2005).

GC analyses were performed using a Hewlett Packard 5890 instrument, equipped with an on-column injector. A fused silica capillary column (50 m × 0.32 mm) coated with CP-Sil-5 (film thickness 0.12 μm) was used with hydrogen as carrier gas and the eluent was monitored by a flame ionization detector. The samples were injected at 50 °C and the oven was programmed to 130 °C at 20 °C/min and then at 4 °C/min to 300 °C at which it was held isothermal for 20 min. The carbon preference index (CPI) was calculated following the method of Schefuß et al. (2003).

GC/MS was performed using a Thermoquest Finnigan TRACE GC, which is equipped with an on-column injector and with helium as the carrier gas, interfaced to a Thermoquest Finnigan TRACE MS operated with electron ionization at 70 eV and scanning a mass range of m/z 50–700 using a cycle time of 1.7 scan s^{-1}. The interface was set to 300 °C with the ion source at 240 °C. The same columns, column conditions and temperature program were used as in the case of the GC analyses. Compounds were identified by comparison of mass spectra and retention time of standards, when possible, or with those reported in the literature.

GC/C/IRMS analysis was performed using a Finnigan Delta-S instrument. The same column, column conditions and temperature program were used as in the case of GC analyses. $\delta^{13}C$ values (reported in standard ‰ notation versus VPDB) were obtained from at least two analyses and the results were averaged to obtain a mean value and to estimate the reproducibility (<5% deviation in the measurements).

HPLC-APCI-MS analyses of the GDGTs were performed using an HP1100 series LC/MS equipped with an auto-injector. The same columns, flow rate and gradient conditions as those described by Hopmans et al. (2004) were used. Detection was achieved using atmospheric pressure positive ion chemical ionization mass spectrometry (APCI-MS) of the eluent using the same conditions as described by Hopmans et al. (2004). GDGTs were detected by single ion monitoring of their $[M+H]^+$ ions (dwell-time = 237 ms) and quantified by integration of the peak areas. The branched and isoprenoid tetraether (BIT) index was calculated following the method of Hopmans et al. (2004).

Total carbon content was determined using a Carlo Erba EA 1108 instrument. The amounts of carbon present as carbonate and sulfur were determined on a Coulomat 702 (Strohlein). The total organic carbon (TOC) contents were determined by subtracting the amounts of carbon present as carbonate from the total amounts of carbon. All values reported are averages of duplicate measurements.

3. RESULTS

3.1. Bulk analyses

The bulk mineralogy, using XRD (Fig. 2), confirms the findings of Bracci et al. (1985). The different ISNs have different abundances of a range of iron sulfide minerals. Greigite is the major constituent of the sample illustrated in Fig. 2a, but pyrite is also abundant. Petrographic observations of polished sections from the ISNs, using an SEM coupled with EDS, indicate that in addition to the two main iron sulfide phases, hexagonal pyrrhotite (Fe_9S_{10}; Fig. 2b–e)

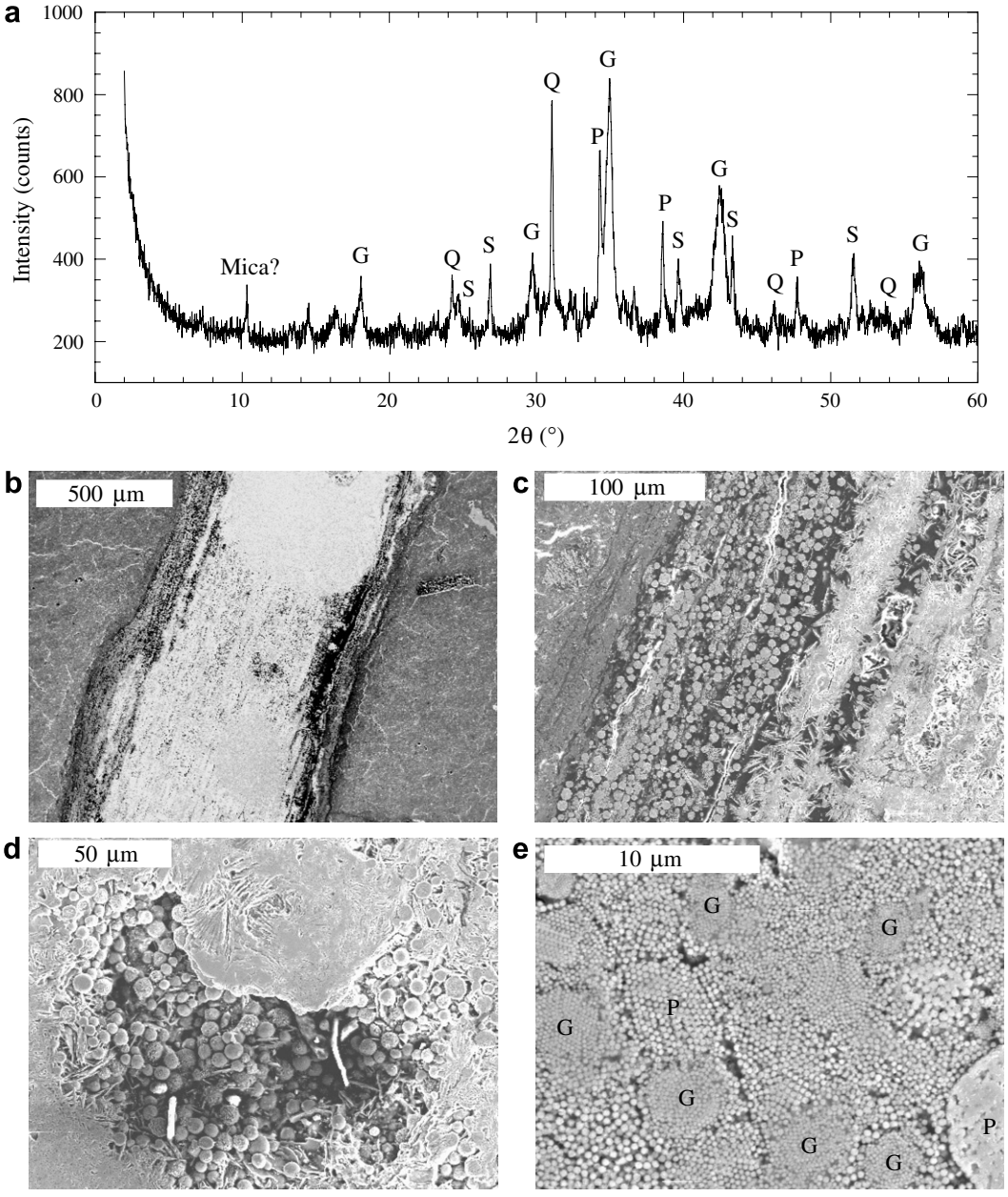

Fig. 2. (a) X-ray diffractogram of a greigite-rich subsample from one of the studied ISNs. G = greigite; P = pyrite; S = elemental sulfur; Q = quartz. (b–e) Back-scattered electron images of an ISN embedded within the host sediment. (b,c) The nodule has an overall linear fabric, which suggests that the iron sulfides have remineralized a pre-existing structure. The arrays of circular (in cross-section) aggregates represent pyrite framboids. The more massive parts of the nodule consist of intergrown plates of hexagonal pyrrhotite. (d) Close-up view of pyrite and greigite framboids with overgrown plates of hexagonal pyrrhotite. (e) Close-up view of an aggregate of pyrite (P) and greigite (G) framboids and less regular space-filling masses of pyrite and greigite. The individual greigite grains are always smaller than the pyrite crystals.

is also present (Fe_9S_{10} is not ferrimagnetic at ambient temperatures). Low magnification views (Fig. 2b) indicate that the iron sulfides have grown in organized bands. Higher magnification views (Fig. 2c and d) indicate that framboidal pyrite was the first phase to grow, probably during early diagenesis, followed by greigite (along with a further generation of pyrite), followed by hexagonal pyrrhotite, which grew around the earlier formed pyrite and greigite. Different sulfidization events are required to produce the observed authigenic growth sequence of these minerals.

Table 1
TOC, total sulfur and carbonate concentration for the analysed iron sulfide nodules

	TOC (%)	TS (%)	Carbonate (%)
ISN A	0.2	26.7	5.2
ISN B	0.2	23.9	3.0
ISN C	0.1	27.8	1.1

The total sulfur contents of the ISNs range between 24% and 28% (Table 1). The TOC and carbonate content range between 0.1% and 0.2% and 1.1% and 5.2%, respectively (Table 1), which indicates that these nodules are relatively organic and carbonate lean.

3.2. Extractable organic matter

3.2.1. Saturated hydrocarbon fractions

GC/MS analyses of the saturated hydrocarbon fractions of all three analysed ISNs revealed predominantly C_{17}–C_{36} *n*-alkanes (Fig. 3a) with C_{29} *n*-alkane (see Appendix, structure I) as the most abundant component and an odd-over-even carbon-number predominance. The $CPIs_{27-33}$ of the *n*-alkanes, ranging from 2.3 to 2.6, are lower than those typically observed for extant plants (CPI > 5), but are typical of relatively immature sediments with higher plant inputs (van Dongen et al., 2006; Mille et al., 2007). Beside these *n*-alkanes, the isoprenoids pristane (II) and phytane (III), steranes (predominantly cholestane (IV)), and hopanes (predominantly 17α,21β(H)-hopane (V)) are present (Fig. 3). Although the distributions are comparable in all three ISNs, these compounds are relatively more abundant in ISNs B and C (Table 2). In addition, in both ISNs B and C, but not in ISN A, a series of unidentified compounds elute between 44 and 47 min. Compound specific isotope analyses indicate that the unidentified compounds are depleted in $\delta^{13}C$, between −79‰ and −101‰. The *n*-alkanes present are not depleted in ^{13}C relative to higher plant biomarkers in other settings, with values between −28‰ and 32‰.

3.2.2. The polar fraction

GC/MS analyses of the polar fractions revealed predominantly C_{13}–C_{30} *n*-alcohols (Fig. 3b and c), with C_{16} *n*-alcohol (VI; ISN A) or C_{18} *n*-alcohol (ISNs B and C) being the most abundant component. In ISNs B and C, C_{31}–C_{35} mid-chain ketones (dipentadecyl, pentadecyl, heptadecyl and diheptadecyl ketones) are also abundant, with C_{33} mid-chain ketone (VII) being predominant. The higher-molecular-weight (>C_{20}) *n*-alcohols have an even-over-odd carbon-number predominance. This is well reflected in the CPI_{26-30} of the *n*-alcohol series, with values of 16.4, 25.7 and 26.9 for ISNs A, B and C, respectively. Beside the *n*-alcohols, substantial amounts of low molecular weight (LMW) *iso*- and *anteiso*-alcohols, predominantly *iso*- and *anteiso*-pentadecanol (C_{15}; VIII and IX), and tentatively identified 10-methylhexadecan-1-ol (X) are also present (Fig. 3c). Compared to the *n*-alcohols, branched *n*-alcohols are much more abundant in ISN A than in ISNs B or C (Table 2).

ISN A also contains substantial amounts of non-isoprenoidal dialkyl glycerol diethers (DGDs), with the C_{33}DGD (dipentadecyl glycerol diether; XI) with two C_{15} alkyl moieties (thought to be *anteiso* branched) and the C_{35} DGD with two C_{16} alkyl moieties (XII) being the most abundant DGDs present. A non-isoprenoidal macrocyclic DGD (XIII) is also present, similar to those identified in acidic geothermal springs (Pancost et al., 2005, 2006). Beside these non-isoprenoidal DGDs, substantial amounts of two macrocyclic isoprenoidal DGDs, containing one or two cyclopentane rings (XIV and XV; Stadnitskaia et al., 2003), archaeol (bis-*O*-phytanyl glycerol diether; XVI) and biphytane diols (XVII and XVIII; Schouten et al., 1998) are also present (Fig. 3b and Fig. 4). The non-isoprenoidal and isoprenoidal DGDs are present in all three studied ISNs, although the concentrations are substantially higher in ISN A than in ISNs B and C (Table 2). The non-isoprenoidal macrocyclic DGD (XIII) and biphytane diols were not observed in ISNs B and C (Table 2).

Other compounds present in the polar fraction of the ISNs include: 3,7,11,15-tetramethylhexadecanol (phytanol; XIX); sterols, predominantly cholesterol (XX); stanols, predominantly ethylcholestanol (XXI); and hopanoids, predominantly bishomohopanol (XXII). However, these compounds are substantially less abundant than the DGDs (Fig. 3b, c and Table 2). Also present are 1,2 and 1,3-diacyl glycerides (DAGs), with the $C_{39:2}$1,3-DAG (XXIII; with a total of 39 carbons and two double bonds) being the most abundant component (Fig. 5). In contrast to ISNs A and B, in which they are only minor components, these are among the most abundant compounds in the polar fraction of ISN C, subordinate only to the *n*-alcohols and ketones (Table 2).

Compound specific isotope analyses of the polar fraction of all studied ISNs indicates that the C_{33} diether (XI) and archaeol (XIV) are both relatively depleted in ^{13}C, with values between −42‰ and −80‰ and −40‰ and −56‰, respectively (note, however, that the C_{33} diether co-elutes with other compounds that appear to be less depleted such that these are maximum $\delta^{13}C$ values). The other compounds present (including marine and terrestrial compounds) have higher $\delta^{13}C$ values that are typical for their inferred sources.

HPLC/MS analyses revealed substantial amounts of intact GDGTs in all ISNs (Fig. 6). The GDGT distributions in the ISNs are dominated by isoprenoidal GDGTs with 0 to 2 cyclopentane rings (XXIV, XXV and XXVI). Substantially smaller amounts of other GDGTs are also present, including crenarchaeol (XXVII) and a suite of non-isoprenoidal branched GDGTs (XXVIII, XXIX and XXX; Fig. 6). The BIT indices (Hopmans et al., 2004) are 0.62, 0.77 and 0.56 for ISN A, B and C, respectively.

4. DISCUSSION

4.1. Depositional environment

Information on the lipid biomarkers preserved in ISNs is limited. Our results illustrate that such lipids can be used to evaluate the depositional environment and microbial assemblages associated with ISN formation. Although there are some differences among the studied ISNs, all three nodules generally have comparable biomarker assemblages. The abundances of biomarkers such as C_{13}–C_{30} *n*-alcohols, with an even-over-odd carbon-number predominance, and C_{17}–C_{36} *n*-alkanes, with an odd-over-even carbon-number predominance and relatively low $\delta^{13}C$ values, indicate that a significant proportion of organic matter in the nodules is terrestrially derived (Eglinton and Hamilton, 1963, 1967).

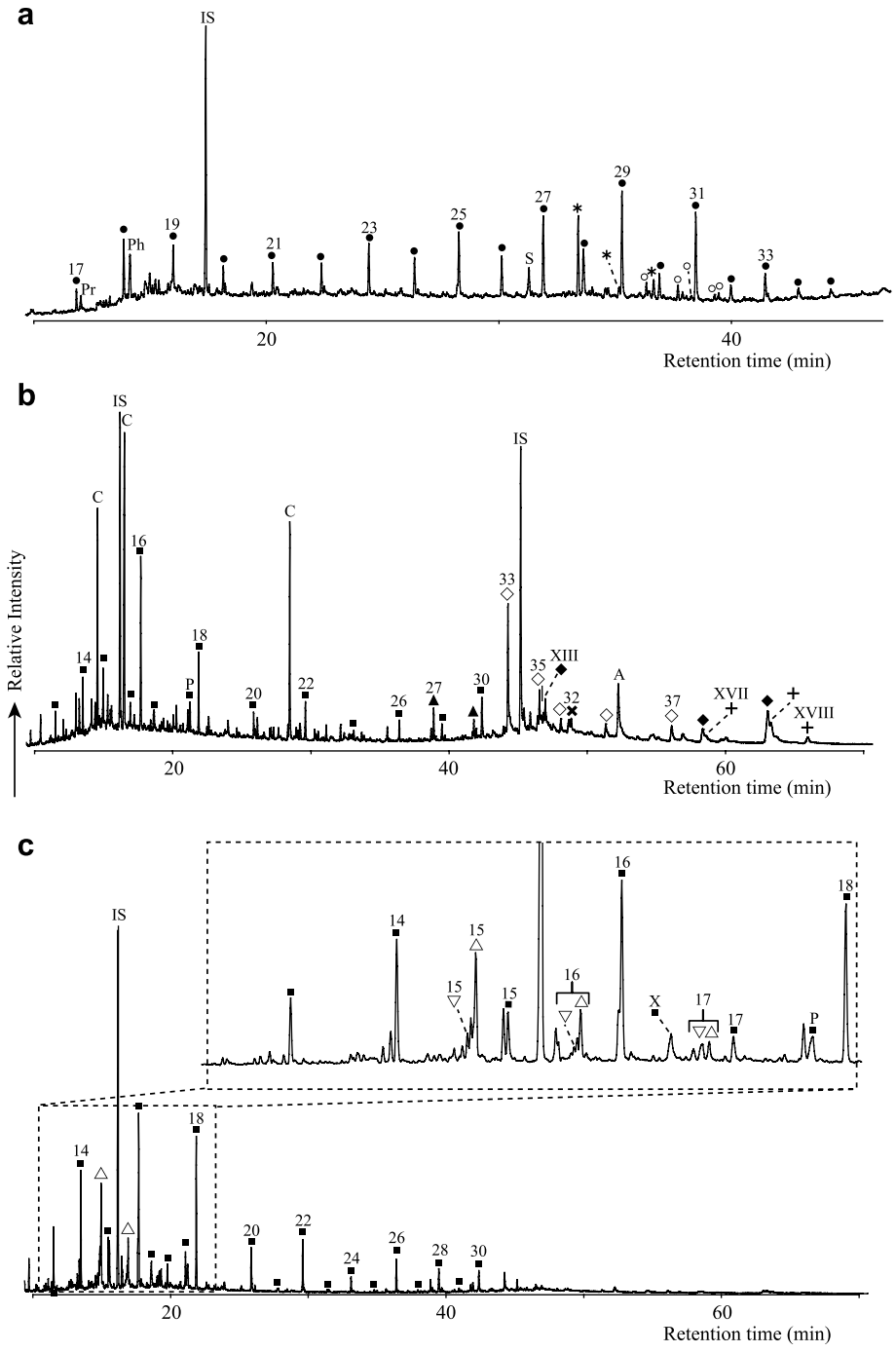

Fig. 3. GC/MS total ion current chromatogram of (a) the saturated hydrocarbon fraction and (b) the polar fraction and (c) the partial m/z 75 mass chromatogram from GC/MS analysis of the polar fraction of iron sulfide nodule A (ISN A). (●) *n*-alkanes, (■) *n*-alcohols, (▽) *iso*-branched alcohols, (△) *anteiso* branched alcohols, (+) biphytane diols, (◇) dialkyl glycerol diethers (DGD), (◆) macrocyclic dialkyl glycerol diethers (DGD), (○) hopanes, (×) hopanoid, (*) steranes, (▲) sterols, Pr = Pristane (II), Ph = Phytane (III), P = 3,7,11,15-tetramethylhexadecanol (phytanol; XIX), A = Archaeol (XVI), IS = standard, S = squalane and C = contaminant. Numbers indicate carbon chain length and ROMAN numerals refer to the compounds shown in the Appendix.

In addition, the BIT index values (>0.5) are typical of sediments receiving high amounts of fluvial terrestrial organic matter (Hopmans et al., 2004; Herfort et al., 2006; Weijers et al., 2006). The surrounding sediments, from which the studied ISNs were sampled, also contain benthic foraminiferal assemblages that are typical of near-shore areas (e.g. Di Bella et al., 2005, and references therein). Thus, the combined evidence suggests formation of the ISNs in a coastal environment dominated by fluvial inputs and higher plant detritus.

Table 2
Concentrations of the major lipid classes in the iron sulfide nodules

Compound (class)	Concentration (ng g^{-1} ISN)		
	ISN A	ISN B	ISN C
Bacterial			
Hopanes[a]	21	96	105
Bishomohopanol	21	6	11
SRB			
Branched *n*-alcohols[b]	301	23	27
DGDs[c]	518	87	159
Macrocyclic DGD XIII	33	n.d.[n]	n.d.[n]
Archaea			
Archeaol	153	18	52
Macrocyclic DGDs[d]	210	26	61
Biphatane diols[e]	164	n.d.[n]	n.d.[n]
Phytanol	33	33	31
Other			
n-Alkanes[f]	266	931	693
n-Alcohols LMW ($<C_{20}$)[g]	581	408	540
n-Alcohols HMW ($>C_{20}$)[h]	227	984	1492
DAGs[i]	22	14	635
Pristane	5	2	1
Phytane	15	31	11
Mid-chain ketones[j]	n.d.[n]	416	847
Steranes[k]	33	60	67
Sterols[l]	65	170	259
Stanols[m]	21	55	92
Squalane	13	35	39
Unidentified compounds in saturated hydrocarbon fraction	n.d.[n]	222	158

[a] The sum of the concentrations of the hopanes from C_{27} till C_{34}; $\Sigma(C_{27} - C_{34})$.
[b] $\Sigma(i + ai(C_{15}–C_{17}) + IX)$.
[c] $\Sigma(C_{33} + C_{34} + C_{35} + C_{35:2} + C_{37:2})$.
[d] $\Sigma(XV + XVI)$.
[e] Σ(XVIII + XIX + an isomer of XIX).
[f] $\Sigma(C_{17}–C_{36})$.
[g] LMW, low molecular weight; $\Sigma(C_{13}–C_{19})$.
[h] HMW, high molecular weight; $\Sigma(C_{20}–C_{30})$.
[i] $\Sigma(C_{37:1} + C_{39:1} + C_{39:2})$.
[j] $\Sigma(C_{31} + C_{33} + C_{35})$.
[k] $\Sigma(C_{27}–C_{29})$.
[l] $\Sigma(C_{27:1}–C_{29:1})$.
[m] $\Sigma(C_{27}–C_{29})$.
[n] n.d., not detected.

4.2. Bacterial and archaeal biomarkers

In addition to the higher plant biomarkers, the presence of substantial amounts of (a) hopanes and hopanols, (b) inferred bacterial DGDs, and (c) archaeal DGDs and GDGTs indicate that microorganisms were also abundant in the environment where these nodules formed. Specifically, the non-isoprenoidal DGDs (Table 2, Fig. 3b and c) have previously been reported in organic-rich settings associated with sulfate reduction and are particularly abundant (and with comparable distributions) in cold seep settings (Pancost et al., 2001a; Werne et al., 2002) where they have been attributed to SRB. This interpretation is supported by the presence of LMW and branched alkanols such as 10-methylhexadecan-1-ol (X). Information about the origin of mid-chain branched alcohols is scarce, but Thiel et al. (1999) found a comparable *n*-alcohol distribution in a Miocene cold seep deposit. Based on isotopic measurements and the observation of Dowling et al. (1986) that 10-methyl branched fatty acids can originate from SRB, Thiel et al. (1999) suggested that these branched alcohols originated from SRB.

GC/MS and LC/MS enabled detection of a variety of archaeal lipids including archaeol, macrocyclic isoprenoidal DGDs bearing one or two cyclopentyl moieties and isoprenoidal GDGTs (Fig. 3b and Fig. 6). Archaeol is a common archaeal membrane lipid (Kates et al., 1993; Koga et al., 1993) found in a variety of settings, but the abundances present in the studied ISNs are comparable to those found in cold seep settings. GDGTs can derive from a wide variety of archaea, including ubiquitous pelagic crenarchaeota. However, such organisms produce predominantly crenarchaeol (XXVII) and GDGT with 0 cyclopentyl moieties (XXIV; Hoefs et al., 1997; Schouten et al., 1998, 2000, 2001; Sinninghe Damsté et al., 2002a,b; Wakeham et al., 2003). In contrast, a distribution dominated by isoprenoidal GDGTs with 0–2 cylcopentyl moieties (XXIV–XXV–XXVI) is comparable to that previously observed in methane seep sediments and carbonate crusts (Pancost et al., 2001b; Aloisi et al., 2002; Zhang et al., 2003; Stadnitskaia et al., 2005). The presence of relatively small amounts of crenarchaeol (XXVII) can probably be attributed to the inclusion of small amounts of planktonic crenarchaeal-derived organic matter during formation of the ISNs. The macrocyclic diethers are less common and have previously been observed only in methane-derived carbonate crusts from the Black Sea (Stadnitskaia et al., 2003, 2005). Other potential archaeal methanotroph compounds present include phytanol and biphytane diols (Schouten et al., 1998; Fig. 3b, and Fig. 4).

4.3. Anaerobic oxidation of methane

Many of the observed archaeal compounds, especially when co-occurring with non-isoprenoidal diethers, have been found in association with AOM (Hinrichs et al., 1999; Elvert et al., 2000; Pancost et al., 2001a,b; Teske et al., 2002; Werne et al., 2002). Stable carbon isotope analyses of these archaeal compounds indicate that they derive from organisms utilizing ^{13}C-depleted methane. We find that both the SRB biomarker C_{33} diether (XI) and the archaeal biomarker archaeol (XVI) are also depleted in ^{13}C, which suggests that these compounds derive from methane-utilizing organisms. The $\delta^{13}C$ values of the diether are comparable to SRB biomarkers that are generally observed in association with methane utilization (Pancost et al., 2000; Peckmann and Thiel, 2004). However, the $\delta^{13}C$ values of methane-utilizing archaeal biomarkers are typically much lower (they can be as low as −124‰; Elvert et al., 2000; Peckmann and Thiel, 2004) than those observed here. Archaeol is a common membrane lipid of different archaeal groups such as halophiles, methanogens and thermophiles (De Rosa and Gambacorta, 1988; De Rosa et al.,

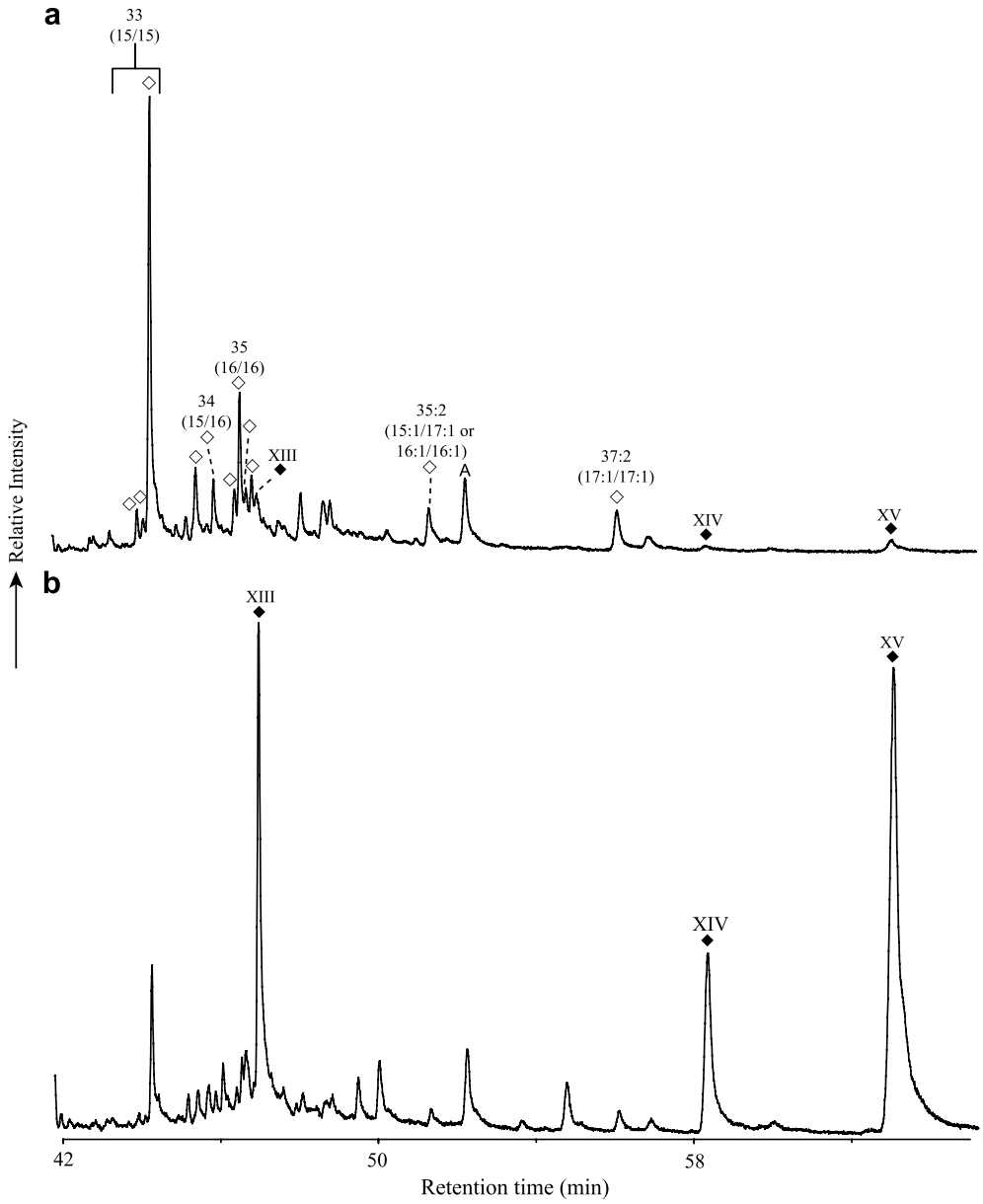

Fig. 4. Partial (a) *m/z* 130 and (b) *m/z* 145 mass chromatograms from GC/MS analysis of the polar fraction of iron sulfide nodule A (ISN A). (◇) Dialkyl glycerol diethers, (◆) macrocyclic dialkyl glycerol diethers, A = Archaeol (XVI). Numbers before the colons indicate carbon chain length, numbers after the colons indicate the number of cyclopentyl moieties and Roman numerals refer to the compounds shown in the Appendix.

1991; Koga et al., 1993), and, although relatively enriched $\delta^{13}C$ values for methane-utilizing archaea biomarkers have been reported before (Teske et al., 2002), the $\delta^{13}C$ values observed here could indicate the mixing of two sources: one from methane-utilizing archaea and the other from non-methane-utilizing organisms. In summary, both the distribution of biomarkers and their carbon isotopic compositions record an AOM signal for all of the studied ISNs.

4.4. AOM processes and the formation of ISNs

The reduction of sulfate coupled to AOM causes an increase in hydrogen sulfide levels (Niewöhner et al., 1998); therefore, AOM was likely to have been closely associated with formation of at least some of the iron sulfide minerals in the studied nodules. Alternatively, the AOM biomarkers could have been generated prior to ISN formation and included in the ISNs in a similar manner as proposed for the planktonic crenarchaeol-derived and terrestrially derived biomarkers. One way to resolve this would be to analyse the surrounding sediments. However, any OM would have been oxidized in the weathered outcrop samples available. Nevertheless, it is unlikely that such high concentrations of AOM biomarkers would have ever been present in the surrounding sediments; the observed concentrations, particularly in ISN A, are much higher than those generally

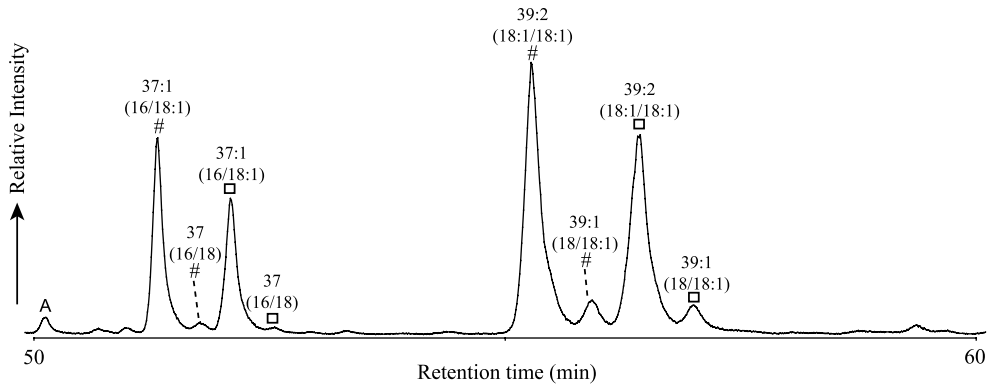

Fig. 5. Partial *m/z* 129 mass chromatogram from GC/MS analysis of the polar fraction of iron sulfide nodule C (ISN C). (#) 1,2-diacyl glycerides, (□) 1,3-diacyl glycerides and A = Archaeol (XVI). Numbers before the colons indicate carbon chain length, numbers after the colons indicate the number of double bonds and the Roman numerals refer to the compound shown in the Appendix.

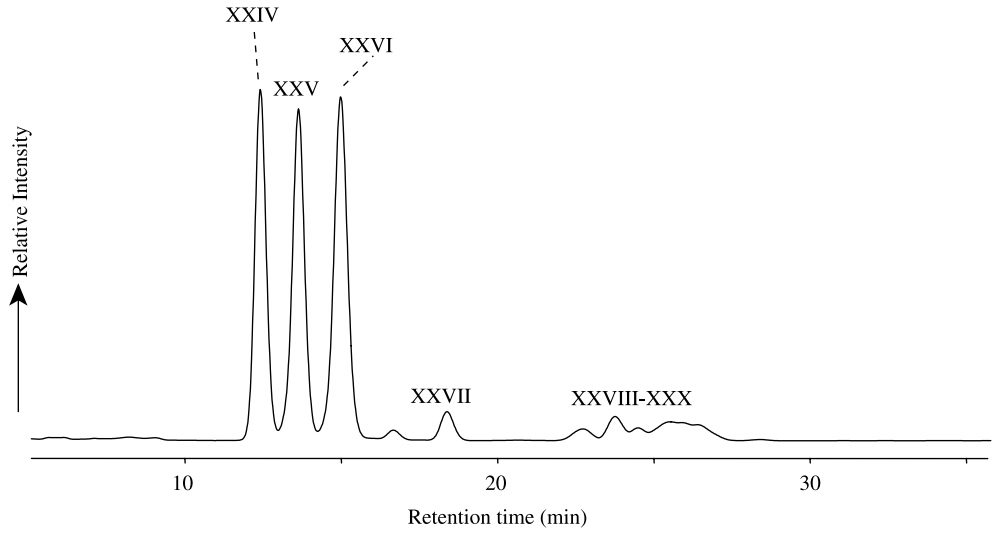

Fig. 6. HPLC/MS base peak chromatogram of tetraether lipids in iron sulfide nodule A. Roman numerals refer to the compounds shown in the Appendix.

observed in other diffusive settings, including those associated with cold seeps (Table 2). For example, the ratio of archaeol to *n*-alkanes (ΣC_{17} to C_{36}) in ISN A (>0.57) is much higher than those generally observed in cores obtained from methane-rich Mediterranean mud volcanoes (<0.095; Werne and Sinninghe Damsté, 2005). Lower abundances of archaeal lipids are also found at the SMTZ in continental margin sediments, where the ratio of archaeal lipids to *n*-alkanes (ΣC_{27}, C_{29}, C_{31} and C_{33}) is <0.2 (Parkes et al., 2007). Thus, AOM appears to be closely linked to the formation of the studied ISNs.

At the SMTZ, the released HS^- reacts with iron oxides resulting in formation of iron sulfide minerals such as pyrite and/or greigite (Kasten et al., 1998; Neretin et al., 2004; Garming et al., 2005; Riedinger et al., 2005). The formation of either pyrite or greigite depends largely on the availability of reactive iron (Kao et al., 2004); if reactive iron is abundant, limited amounts of hydrogen sulfide will react with the iron and pyritization reactions will not proceed to completion, thereby enabling preservation of greigite. It is unclear how pyrite can form at depth in this type of sediment (Burdige, 2006), although if hydrogen sulfide is abundant at depth, it could conceivably react with detrital iron to form pyrite via iron monosulfide precursors. Regardless, there is considerable evidence that greigite can form long after early burial (e.g. Roberts and Weaver, 2005; Rowan and Roberts, 2006). Based on our results, two scenarios are possible for the formation of the ISNs. In the first, framboidal pyrite formed at shallow depths within the sediment column as a consequence of sulfate reduction coupled to OM oxidation. The pyrite then acted as a site for preferred crystallization of greigite (along with further generation of pyrite) at the SMTZ. A similar process has been proposed to occur at the SMTZ of Amazon Fan sediments. There, greigite formation occurs without transformation to the diagenetic end-product pyrite (Kasten et al., 1998); this has been attributed to high iron concentrations that consumed H_2S before full reaction to pyrite could occur. This is possible within the Valle Ricca sediments, with formation of hexagonal pyrrhotite around

the greigite occurring during later burial. Several studies of recent sediments have made a similar association between greigite precipitation and AOM (Kates et al., 1993; Niewöhner et al., 1998; Neretin et al., 2004; Garming et al., 2005; Riedinger et al., 2005; Larrasoaña et al., 2007). However, in this model, ISN formation does not *a priori* require AOM, and it is likely that AOM is not always associated with ISN formation in other settings.

In a second alternative for the formation of the ISNs, the relative concentration of HS^- compared to reactive iron could have been high, such that frambodial pyrite precipitated at the SMTZ, capturing the AOM biomarker signature. At greater depths, iron sulfide continued to precipitate, but due to the relatively low concentration of hydrogen sulfide, mainly greigite was formed. Similar to the first scenario, this scenario is followed by formation of hexagonal pyrrhotite around the greigite at a later stage. Unfortunately, we could not characterize biomarker assemblages that are specifically associated with either the greigite or pyrite components of the ISNs; thus, we cannot exclude this scenario. However, this second scenario seems less likely than the first alternative described above for several reasons. First, in nearshore, coastal environments, sulfate reduction is coupled to shallow OM degradation such that pyrite will have almost certainly precipitated at depths shallower than the SMTZ. Second, below the SMTZ, sulfate is depleted and OM degradation proceeds by fermentation coupled to methanogenesis, neither of which are sulfide-producing processes (Burdige, 2006), which makes it difficult to understand how greigite could form at such depths. Nevertheless, in both models, methane-driven sulfate reduction has played a key role in the formation of these ISNs, with either concurrent or subsequent greigite formation.

4.5. Implications for the paleomagnetic record

Either of the above scenarios will have a significant impact on the paleomagnetic record. Pyrite formation will have occurred at the expense of the magnetic iron oxides present, which will have reduced the magnetization of the sediments (e.g. Karlin and Levi, 1983; Canfield and Berner, 1987; Channell and Hawthorne, 1990; Karlin, 1990; Passier et al., 1998), while greigite, which is ferrimagnetic, will have produced a strong secondary paleomagnetic signal (e.g. Jiang et al., 2001; Roberts and Weaver, 2005; Sagnotti et al., 2005; Rowan and Roberts, 2006). Global methane production in marine sediments is significant and is estimated between 75 and 320 Tg $year^{-1}$ (Kvenvolden, 1988; Valentine, 2002; Parkes et al., 2007). The main factor controlling the formation of greigite in the AOM zone is the interplay between the rates of downward sulfate and upward methane diffusion, which in turn controls the amount of sulfide produced (Kasten et al., 1998; Neretin et al., 2004; Larrasoaña et al., 2007). Consequently, upward migration of methane and subsequent AOM in marine sediments can have a profound impact on paleomagnetic records. In addition, the widespread occurrence of methane migration in sediments suggests that associated diagenetic formation of iron sulfides provides a widespread mechanism for the common remagnetizations reported in association with sedimentary greigite (e.g. Florindo and Sagnotti, 1995; Horng et al., 1998; Jiang et al., 2001; Roberts and Weaver, 2005; Rowan and Roberts, 2006).

The formation of ISNs is probably dependant on the ratio of available reactive iron relative to hydrogen sulfide concentrations. Generally, low quantities of hydrogen sulfide relative to reactive iron favors formation of greigite, whereas higher hydrogen sulfide concentrations favor formation of the more stable pyrite (Kao et al., 2004). The former situation is unlikely to occur at most cold seeps, where rates of AOM—and sulfide concentrations—are high. Instead, in agreement with recent analyses of nodular sulfides in gas hydrate bearing sediments from Ocean Drilling Program Leg 204 (Larrasoaña et al., 2007), we suggest that this process is more likely to occur in diffusive methane flux settings in continental margin sediments with high quantities of reactive iron.

5. CONCLUSIONS

(1) Organic geochemical analyses of iron sulfide nodules reveal a biomarker composition that is consistent with their formation in a coastal marine setting in association with sulfate reducing bacteria and methanotrophic archaea.
(2) The reduction of sulfate associated with anaerobic oxidation of methane would have caused increases in pore water sulfide concentrations; this sulfide would have been available to react with iron oxides, and could have played a role in the formation of iron sulfide nodules that contain greigite. Regardless of its origin, this diagenetic growth of greigite occurred at a sufficiently late stage to remagnetize the sediments.
(3) If the above process is widespread, then the upward migration of methane in marine sediments could have a profound impact on paleomagnetic records.

ACKNOWLEDGEMENTS

We thank Dr. Ian D. Bull, Dr Rob Berstan, Martijn Woltering and Dr. Ellen Hopmans for technical assistance, NERC for funding the Bristol node of the Life Sciences Mass Spectrometry Facility (Agreement No. F14/6/13/01; http://www.chm.bris.ac.uk/lsmsf/index.html) and for financial support to B. van Dongen (grant NER/A/S/2001/01213), Luke Handley for preparing the samples for GDGT analysis and Dr. David Burdige (Associate Editor) and Dr. D. Valentine and two anonymous reviewers for comments that improved the manuscript.

APPENDIX A. SUPPLEMENTARY DATA

Supplementary data associated with this article can be found, in the online version, at doi:10.1016/j.gca.2007.08.019.

REFERENCES

Aloisi G., Bouloubassi I., Heijs S. K., Pancost R. D., Pierre C., Sinninghe Damsté J. S., Gottschal J. C., Forney L. J. and

Rouchy (2002) CH_4-consuming microorganisms and the formation of carbonate crusts at cold seeps. *Earth Planet. Sci. Lett.* **203**, 195–203.

Berner R. A. (1970) Sedimentary pyrite formation. *Am. J. Sci.* **268**, 1–23.

Boetius A., Ravenschlag K., Schubert C. J., Rickert D., Widdel F., Gieseke A., Amann R., Jørgensen B. B., Witte U. and Pfannkuche O. (2000) A marine microbial consortium apparently mediating anaerobic oxidation of methane. *Nature* **407**, 623–626.

Borzi M., Carboni M. G., Cilento G., Di Bella L., Florindo F., Girotti O., Piccardi E. and Sagnotti L. (1998) Bio- and magneto-stratigraphy in the Tiber Valley revised. *Quat. Int.* **47–48**, 65–72.

Bracci G., Dalena D. and Orlandi P. (1985) La greigite di Mentana, Lazio. *Rend. Soc. Ital. Mineral. Petrol.* **40**, 295–298.

Burdige D. J. (2006) *Geochemistry of Marine Sediments*. Princeton University Press, Princeton and Oxford.

Canfield D. E. and Berner R. A. (1987) Dissolution and pyritization of magnetite in anoxic marine sediments. *Geochim. Cosmochim. Acta* **51**, 645–659.

Channell J. E. T. and Hawthorne T. (1990) Progressive dissolution of titanomagnetites at ODP Site 653 (Tyrrhenian Sea). *Earth Planet. Sci. Lett.* **96**, 469–480.

De Rosa M. and Gambacorta A. (1988) The lipids of archaebacteria. *Prog. Lipid Res.* **27**, 153–175.

De Rosa M., Trincone A., Nicolaus B. and Gambacorta A. (1991) Archaebacteria: lipids, membrane structures, and adaptation to environmental stresses. In *Life Under Extreme Conditions* (ed. G. Di Prisco). Springer-Verlag, Berlin, pp. 61–87.

Devol A. H. and Ahmed S. I. (1981) Are high rates of sulphate reduction associated with anaerobic oxidation of methane? *Nature* **291**, 407–408.

Di Bella L., Carboni M. G., Bergamin L. and Iamundo F. (2005) The Early Pleistocene in Latium (Central Italy): palaeoecology from benthic foraminiferal record. *Quat. Int.* **131**, 23–34.

Dowling N. J. E., Widdel F. and White D. C. (1986) Phospholipid ester-linked fatty-acid biomarkers of acetate-oxidizing sulfate-reducers and other sulfide-forming bacteria. *J. Gen. Microbiol.* **132**, 1815–1825.

Eglinton G. and Hamilton R. J. (1963) The distribution of *n*-alkanes. In *Chemical Plant Taxonomy* (ed. T. Swain). Academic Press, pp. 187–217.

Eglinton G. and Hamilton R. J. (1967) Leaf epicuticular waxes. *Science* **156**, 1322–1335.

Elvert M., Suess E., Greinert J. and Whiticar M. J. (2000) Archaea mediating anaerobic methane oxidation in deep-sea sediments at cold seeps of the eastern Aleutian subduction zone. *Org. Geochem.* **31**, 1175–1187.

Florindo F. and Sagnotti L. (1995) Palaeomagnetism and rock magnetism in the upper Pliocene Valle Ricca (Rome, Italy) section. *Geophys. J. Int.* **123**, 340–354.

Garming J. F. L., Bleil U. and Riedinger N. (2005) Alteration of magnetic mineralogy at the sulfate-methane transition: Analysis of sediments from the Argentine continental slope. *Phys. Earth Planet. Inter.* **151**, 290–308.

Goldhaber M. B. (2003) Sulfur-rich Sediments. In *Treatise on Geochemistry, Sediments Diagenesis and Sedimentary Rocks*, vol. 7 (eds. F. T. Mackenzie, H. D. Holland and K. K. Turekian). Elsevier, pp. 257–288.

Herfort L., Schouten S., Boon J. P. and Sinninghe Damsté J. S. (2006) Application of the TEX86 temperature proxy to the southern North Sea. *Org. Geochem.* **37**, 1715–1726.

Hinrichs K. U., Hayes J. M., Sylva S. P., Brewer P. G. and DeLong E. F. (1999) Methane-consuming archaebacteria in marine sediments. *Nature* **398**, 802–805.

Hinrichs K. U., Summons R. E., Orphan V., Sylva S. P. and Hayes J. M. (2000) Molecular and isotopic analysis of anaerobic methane-oxidizing communities in marine sediments. *Org. Geochem.* **31**, 1685–1701.

Hoefs M. J. L., Schouten S., De Leeuw J. W., King L. L., Wakeham S. G. and Sinninghe Damsté J. S. (1997) Ether lipids of planktonic archaea in the marine water column? *Appl. Environ. Microbiol.* **63**, 3090–3095.

Hopmans E. C., Weijers J. W. H., Schefuss E., Herfort L., Sinninghe Damsté J. S. and Schouten S. (2004) A novel proxy for terrestrial organic matter in sediments based on branched and isoprenoid tetraether lipids. *Earth Planet. Sci. Lett.* **224**, 107–116.

Horng C.-S., Torii M., Shea K.-S. and Kao S.-J. (1998) Inconsistent magnetic polarities between greigite- and pyrrhotite/magnetite-bearing marine sediments from the Tsailiao-chi section, southwestern Taiwan. *Earth Planet. Sci. Lett.* **164**, 467–481.

Jiang W.-T., Horng C.-S., Roberts A. P. and Peacor D. R. (2001) Contradictory magnetic polarities in sediments and variable timing of neoformation of authigenic greigite. *Earth Planet. Sci. Lett.* **193**, 1–12.

Kao S.-J., Horng C.-S., Roberts A. P. and Liu K.-K. (2004) Carbon–sulfur–iron relationships in sedimentary rocks from southwestern Taiwan: Influence of geochemical environment on greigite and pyrrhotite formation. *Chem. Geol.* **203**, 153–168.

Karlin R. (1990) Magnetite diagenesis in marine sediments from the Oregon continental margin. *J. Geophys. Res.* **95**, 4405–4419.

Karlin R. and Levi S. (1983) Diagenesis of magnetic minerals in recent haemipelagic sediments. *Nature* **303**, 327–330.

Karlin R. and Levi S. (1985) Geochemical and sedimentological control of the magnetic properties of hemipelagic sediments. *J. Geophys. Res.* **90**, 10373–10392.

Kasten S., Freudenthal T., Gingele F. X. and Schulz H. D. (1998) Simultaneous formation of iron-rich layers at different redox boundaries in sediments of the Amazon deep-sea fan. *Geochim. Cosmochim. Acta* **62**, 2253–2264.

Kates M., Kushner D. J. and Matheson A. T. (1993) *The biochemistry of Archaea (Archaebacteria)*. Elsevier, Amsterdam.

Koga Y., Akagawa-Matsushita M., Ohga M. and Nishihara M. (1993) Taxonomic significance of the distribution of component parts of polar ether lipids in methanogens. *Syst. Appl. Microbiol.* **16**, 342.

Kvenvolden K. A. (1988) Methane hydrate—a major reservoir of carbon in the shallow geosphere? *Chem. Geol.* **71**, 41–51.

Larrasoaña J. C., Roberts A. P., Musgrave R. J., Gràcia E., Piñero E., Vega M. and Martínez-Ruiz F. (2007) Diagenetic formation of greigite and pyrrhotite in marine sedimentary systems containing gas hydrates. *Earth Planet. Sci. Lett.* **261**, 350–366.

Mille G., Asia L., Guiliano M., Malleret L. and Doumenq P. (2007) Hydrocarbons in coastal sediments from the Mediterranean Sea (Gulf of Fos area, France). *Mar. Pollut. Bull.* **54**, 566–575.

Murray J. W., Grundmanis V., Smethie J. and William M. (1978) Interstitial water chemistry in the sediments of Saanich Inlet. *Geochim. Cosmochim. Acta* **42**, 1011–1026.

Neretin L. N., Böttcher M. E., Jørgensen B. B., Volkov I. I., Luschen H. and Hilgenfeldt K. (2004) Pyritization processes and greigite formation in the advancing sulfidization front in the upper Pleistocene sediments of the Black Sea. *Geochim. Cosmochim. Acta* **68**, 2081–2093.

Niewöhner C., Hensen C., Kasten S., Zabel M. and Schulz H. D. (1998) Deep sulfate reduction completely mediated by anaerobic methane oxidation in sediments of the upwelling area off Namibia. *Geochim. Cosmochim. Acta* **62**, 455–464.

Orcutt B., Boetius A., Elvert M., Samarkin V. and Joye S. B. (2005) Molecular biogeochemistry of sulfate reduction, methanogenesis and the anaerobic oxidation of methane at Gulf of Mexico cold seeps. *Geochim. Cosmochim. Acta* **69**, 4267–4281.

Pancost R. D., Bouloubassi I., Aloisi G. and Sinninghe Damsté J. S.The Medinaut Shipboard Scientific Party (2001a) Three series of non-isoprenoidal dialkyl glycerol diethers in cold-seep carbonate crusts. *Org. Geochem.* **32**, 695–707.

Pancost R. D., Hopmans E. C. and Sinninghe Damsté J. S. (2001b) Archaeal lipids in Mediterranean cold seeps: molecular proxies for anaerobic methane oxidation. *Geochim. Cosmochim. Acta* **65**, 1611–1627.

Pancost R. D., Pressley S., Coleman J. M., Benning L. G. and Mountain B. W. (2005) Lipid biomolecules in silica sinters: indicators of microbial biodiversity. *Environ. Microbiol.* **7**, 66–77.

Pancost R. D., Pressley S., Coleman J. M., Talbot H. M., Kelly S. M., Farrimond P., Schouten S., Benning L. and Mountain B. W. (2006) Composition and implications of diverse lipids in NZ hydrothermal sinters. *Geobiology* **4**, 71–92.

Pancost R. D. and Sinninghe Damsté J. S. (2003) Life at cold seeps: a synthesis of biogeochemical and ecological data from Kazan mud volcano, eastern Mediterranean Sea. *Chem. Geol.* **205**, 367–390.

Pancost R. D., Sinninghe Damsté J. S., de Lint S., van der Maarel M. J. E. C. and Gottschal J. C. The Medinaut Shipboard Scientific Party (2000) Biomarker evidence for widespread anaerobic methane oxidation in Mediterranean sediments by a consortium of methanogenic archaea and bacteria. *Appl. Environ. Microbiol.* **66**, 1126–1132.

Parkes R. J., Cragg B. A., Banning N., Brock F., Webster G., Fry J. C., Hornibrook E., Pancost R. D., Kelly S., Knab N., Jørgensen B. B., Rinna J. and Weightman A. J. (2007) Biogeochemistry and biodiversity of methane cycling in subsurface marine sediments (Skagerrak, Denmark). *Environ. Microbiol.* **9**, 1146–1161.

Passier H. F., Dekkers M. J. and de Lange G. J. (1998) Sediment chemistry and magnetic properties in an anomalously reducing core from the eastern Mediterranean Sea. *Chem. Geol.* **152**, 287–306.

Peckmann J. and Thiel V. (2004) Carbon cycling at ancient methane-seeps. *Chem. Geol.* **205**, 443–467.

Riedinger N., Pfeifer K., Kasten S., Garming J. F. L., Vogt C. and Hensen C. (2005) Diagenetic alteration of magnetic signals by anaerobic oxidation of methane related to a change in sedimentation rate. *Geochim. Cosmochim. Acta* **69**, 4117–4126.

Roberts A. P. and Turner G. M. (1993) Diagenetic formation of ferrimagnetic iron sulphide minerals in rapidly deposited marine sediments, South Island, New Zealand. *Earth Planet. Sci. Lett.* **115**, 257–273.

Roberts A. P. and Weaver R. (2005) Multiple mechanisms of remagnetization involving sedimentary greigite (Fe_3S_4). *Earth Planet. Sci. Lett.* **231**, 263–277.

Rowan C. J. and Roberts A. P. (2006) Magnetite dissolution, diachronous greigite formation, and secondary magnetizations from pyrite oxidation: Unravelling complex magnetizations in Neogene marine sediments from New Zealand. *Earth Planet. Sci. Lett.* **241**, 119–137.

Sagnotti L., Roberts A. P., Weaver R., Verosub K. L., Florindo F., Pike C. R., Clayton T. and Wilson G. S. (2005) Apparent magnetic polarity reversals due to magnetization resulting from late diagenetic growth of greigite from siderite. *Geophys. J. Int.* **160**, 89–100.

Schefuß E., Ratmeyer V., Stuut J. B. W., Jansen J. H. F. and Sinninghe Damsté J. S. (2003) Carbon isotope analyses of *n*-alkanes in dust from the lower atmosphere over the central eastern Atlantic. *Geochim. Cosmochim. Acta* **67**, 1757–1767.

Schouten S., Hoefs M. J. L., Koopmans M. P., Bosch H. J. and Sinninghe Damsté J. S. (1998) Structural characterization, occurrence and fate of archaeal ether-bound acyclic and cyclic biphytanes and corresponding diols in sediments. *Org. Geochem.* **29**, 1305–1320.

Schouten S., Hopmans E. C., Pancost R. D. and Sinninghe Damsté J. S. (2000) Widespread occurrence of structurally diverse tetraether membrane lipids: Evidence for the ubiquitous presence of low-temperature relatives of hyperthermophiles. *Proc. Natl. Acad. Sci.* **97**, 14421–14426.

Schouten S., Wakeham S. G. and Sinninghe Damsté J. S. (2001) Evidence for anaerobic methane oxidation by archaea in euxinic waters of the Black Sea. *Org. Geochem.* **32**, 1277–1281.

Sinninghe Damsté J. S., Rijpstra W. I. C., Hopmans E. C., Prahl F. G., Wakeham S. G. and Schouten S. (2002a) Distribution of membrane lipids of planktonic crenarchaeota in the Arabian Sea. *Appl. Environ. Microbiol.* **68**, 2997–3002.

Sinninghe Damsté J. S., Schouten S., Hopmans E. C., van Duin A. C. T. and Geenevasen J. A. J. (2002b) Crenarchaeol: The characteristic core glycerol dibiphytanyl glycerol tetraether membrane lipid of cosmopolitan pelagic crenarchaeota. *J. Lipid Res.* **43**, 1641–1651.

Skinner B. J., Erd R. C. and Grimaldi F. S. (1964) Greigite, the thio-spinel of iron; a new mineral. *Am. Mineral.* **49**, 543–555.

Stadnitskaia A., Bass M., Ivanov M. K., van Weering T. C. E. and Sinninghe Damsté J. S. (2003) Novel archaeal macrocyclic diether core membrane lipids in a methane-derived carbonate crust from a mud volcano in the Sorokin Trough, NE Black Sea. *Archaea* **1**, 165–174.

Stadnitskaia A., Muyzer G., Abbas B., Coolen M. J. L., Hopmans E. C., Baas M., van Weering T. C. E., Ivanov M. K., Poludetkina E. and Sinninghe Damsté J. S. (2005) Biomarker and 16S rDNA evidence for anaerobic oxidation of methane and related carbonate precipitation in deep-sea mud volcanoes of the Sorokin Trough, Black Sea. *Mar. Geol.* **217**, 67–96.

Teske A., Hinrichs K. U., Edgcomb V., de Vera Gomez A., Kysela D., Sylva S. P., Sogin M. L. and Jannasch H. W. (2002) Microbial diversity of hydrothermal sediments in the Guaymas Basin: Evidence for anaerobic methanotrophic communities. *Appl. Environ. Microbiol.* **68**, 1994–2007.

Thiel V., Peckmann J., Richnow H. H., Luth U., Reitner J. and Michaelis W. (2001) Molecular signals for anaerobic methane oxidation in Black Sea seep carbonates and a microbial mat. *Mar. Chem.* **73**, 97–112.

Thiel V., Peckmann J., Seifert R., Wehrung P., Reitner J. and Michaelis W. (1999) Highly isotopically depleted isoprenoids: Molecular markers for ancient methane venting. *Geochim. Cosmochim. Acta* **63**, 3906–3959.

Valentine D. L. (2002) Biogeochemistry and microbial ecology of methane oxidation in anoxic environments: a review. *Anton. Leeuw. Int. J. G.* **81**, 271–282.

van Dongen B. E., Talbot H. M., Schouten S., Pearson P. N. and Pancost R. D. (2006) Well preserved Palaeogene and Cretaceous biomarkers from the Kilwa area, Tanzania. *Org. Geochem.* **37**, 539–557.

Wakeham S. G., Lewis C. M., Hopmans E. C., Schouten S. and Sinninghe Damsté J. S. (2003) Archaea mediate anaerobic oxidation of methane in deep euxinic waters of the Black Sea. *Geochim. Cosmochim. Acta* **67**, 1359–1374.

Weaver R., Roberts A. P. and Barker A. J. (2002) A late diagenetic (syn/folding) magnetization carried by pyrrhotite: Implications for paleomagnetic studies from magnetic iron sulphide-bearing sediments. *Earth Planet. Sci. Lett.* **3–4**, 371–386.

Weijers J. W. H., Schouten S., Spaargaren O. C. and Sinninghe Damsté J. S. (2006) Occurrence and distribution of tetraether

membrane lipids in soils: Implications for the use of the Tex_{86} proxy and the BIT index. *Org. Geochem.* **37**, 1680–1693.

Werne J. P., Baas M. and Sinninghe Damsté J. S. (2002) Molecular isotopic tracing of carbon flow and trophic relationships in a methane-supported benthic microbial community. *Limnol. Oceanogr.* **47**, 1694–1701.

Werne J. P., Haese R. R., Zitter T., Aloisi G., Bouloubassi I., Heijs S., Fiala-Medioni A., Pancost R. D., Sinninghe Damsté J. S. and de Lange G. (2004) Life at cold seeps: a synthesis of biogeochemical and ecological data from Kazan mud volcano, eastern Mediterranean Sea. *Chem. Geol.* **205**, 367–390.

Werne J. P. and Sinninghe Damsté J. S. (2005) Mixed sources contribute to the molecular isotopic signature of methane-rich mud breccia sediments of Kazan mud volcano (eastern Mediterranean). *Org. Geochem.* **36**, 13–27.

Zhang C. L., Pancost R. D., Sassen R., Qian Y. and Macko S. A. (2003) Archaeal lipid biomarkers and isotopic evidence of anaerobic methane oxidation associated with gas hydrates in the Gulf of Mexico. *Org. Geochem.* **34**, 827–836.

Associate editor: David J. Burdige